Defects in Qswitched laser annealed silicon

K. L. Wang, Y. S. Liu, G. E. Possin, J. Karins, and J. Corbett

Citation: J. Appl. Phys. **54**, 3839 (1983); doi: 10.1063/1.332608

View online: http://dx.doi.org/10.1063/1.332608

View Table of Contents: http://jap.aip.org/resource/1/JAPIAU/v54/i7

Published by the American Institute of Physics.

Defects in Q-switched laser annealed silicon

K. L. Wang
Device Research Laboratory, Electrical Engineering Department, University of California, Los Angeles, California 90024

Y. S. Liu and G. E. Possin
General Electric Corporate Research and Development Center, Schenectady, New York 12345

J. Karins, Jr.[a] and J. Corbett
State University of New York, Albany, New York 12222

(Received 20 October 1982; accepted for publication 13 January 1983)

This paper describes the characterization of residual defects using transient capacitance spectroscopy for ion-implanted Si annealed with a Q-switched Nd-glass laser. The deep-level defect levels observed in this study were similar to those obtained in low-fluence ion implanted samples. The spatial distributions of deep-level defect concentrations were obtained for conditions using different anneal energy densities. From the difference of the distribution profiles, it is concluded that the greater the annealing laser energy densities, the lower the defect concentration near the junction.The reduction of the defect concentration is partly due to the inward movement of the junction. Thus the defects detected are those which lie further down in the tail of the defect distribution profile and have a lower concentration. Other reasons for the reduction of the defect concentration can be due to thermal annealing as heat propagates into the substrate during laser radiation. The reduction of the defect concentration agrees with the improvement of the measured I–V characteristics. Annealing with multiple shots of laser radiation was performed and the annealing model was established. The junction movement was confirmed by an electron beam induced conductivity technique. The carrier diffusion length measured in the region, where a surface layer of 2–3 μm was etched, decreases as the annealing energy density increases. This may be explained by the fact that the native defects generated thermally in the melts at the surface diffuse into the bulk and subsequently are trapped by the impurities in Si.

PACS numbers: 61.70. – r

I. INTRODUCTION

The use of high power laser irradiation in annealing ion-implanted Si has received a great deal of attention.[1–4] The recovery of crystallinity from the ion-damaged amorphous layer has been studied extensively using transmission electron microscopy (TEM)[5,6] and Rutherford backscattering spectroscopy (RBS).[7,8] However the leakage current in many cases has not been shown to correlate with the deep-level defects. In a study of laser irradiation of virgin Si, Kimerling and Benton observed that the concentrations of the laser-processed induced defects increased with the annealing energy densities.[10,11] This result appears to contradict those of the reverse bias leakage current measurements. In addition, the origins of many observed defects after laser annealing or processing remain controversial.[12–15]

This paper describes a detailed study of residual defects in ion-implanted silicon which has been subjected to pulsed laser annealing. Deep-level transient spectroscopy (DLTS) is used to determine the energy levels and the defect concentrations. The concentrations of the defects are compared with the reverse bias leakage current density. In some cases an additional low temperature thermal anneal is necessary in order to achieve a low leakage in the diodes. The leakage current, residual deep-level defects, and their spatial distributions are presented and discussed for samples laser annealed with various energy densities. The reduction of deep-level point defects as the laser energy density and the number of irradiation pulses increases is explained.

II. EXPERIMENTAL DESCRIPTION

The silicon wafers used were commercially available polished and dislocation-free Czochralski (CZ) and floating zone (FZ) materials. Both n- and p-type Si in ⟨111⟩ and ⟨100⟩ orientations with a resistivity of about 4 Ω cm were used for experiments. Ion implantation was carried out with $^{75}As^+$ or $^{28}Si^+$ at 78 and 297 K. The wafers were tilted 7° during ion implantation in order to avoid channeling along major axes. The annealing laser was a Q-switched Nd:glass oscillator and an amplifier ($\lambda = 1.06\,\mu$m). The oscillator was operated in TEM mode with a constant energy output and a pulse width of 80 ns (FWHM).By varying the amplifier gain, the energy density of the laser pulse incident upon the sample could be adjusted over a range of 1–8 J cm^{-2} on a 1-cm^2 area. Samples were irradiated at nearly normal incidence. Mesa diodes of 1.1×10^{-3} cm^2 in area were fabricated from As^+-implanted p-type samples after laser annealing while Schottky diodes were fabricated from Si^+-implanted samples.

The melting of the Si surface with a pulsed laser having a sufficient energy density is well established[16,17] and the signature of the enhanced reflected waveform as a result of

[a] Phillips Laboratories, 345 Scarborough Road, Briarcliff Manor, NY 10510.

 0021-8979/83/073839-10$02.40

the first laser pulse indicates the melting of the silicon. Details of the experiment are discussed in a previous publication.[17] As described in that publication, the enhancement of reflectivity is a direct indication of surface melting upon laser irradiation. For As implants at 90 KeV with a fluence of 8×10^{15} As cm^{-2}, the threshold energy densities determined by this technique were 2.4 and 2.7 J cm^{-2} for 78 and 300 K implantation temperatures, respectively.

III. EXPERIMENTAL RESULTS AND DISCUSSION

A. Diode characteristics

The reverse leakage current of mesa diodes fabricated from the laser-annealed material was measured. For the $^{75}As^{+}$ implants at 300K, with a fluence of 8×10^{15} cm^{-2} at 90 KeV, Fig. 1 illustrates the reverse leakage current density for an array of diodes fabricated in regions irradiated with three different irradiation energy densities. The three different energy densities 2.3, 2.7, and 3.2 J cm^{-2}, corresponded to the values below, just above, and well above the required energy threshold. It is noted that even though the implanted amorphous layer had recrystallized after annealing with an energy density of $E = 2.7$ J cm^{-2}, the fabricated diodes were very leaky. The annealing energy density required for achieving low leakage current is about 3.2 J cm^{-2} or greater. The fine features of the spatial leakage current distributions of the diodes were shown in Fig. 1 and were due to some nonuniformity of the laser output as reported earlier.

The I–V characteristics of the sample laser annealed with $E = 3.2$ J cm^{-2} were compared with those of a sample thermally annealed at 920 °C in Ar ambient. The reverse leakage current of the laser-annealed diodes is slightly lower than that of thermally annealed diodes. However, the forward current characteristics for both kinds of samples are comparable and give a diode ideality factor of 1.06, which indicates a low defect concentration in the implanted region. For implants carried out at higher energies but under otherwise the same conditions, the same annealing energy density used for the 90-KeV implant is not sufficient to reduce the diode leakage current density to that comparable with the thermal annealing data. The corresponding leakage currents shown in Fig. 2 are much higher than those shown in Fig. 1. This can be explained by the longer damage range created by higher energy ions. A greater melting depth is required to recrystallize the damaged Si and subsequently a deeper junction forms for low leakage diodes as will be discussed later. Similarly, different implantation temperatures required different annealing energy densities for yielding low-leakage diodes since the damage depth changes with implant temperature. For the implants carried out at 78 °K, a thicker amorphous layer resulted and a higher laser energy density is necessary for obtaining low leakage diodes. For example, an energy density greater than 5 J cm^{-2} is required for samples implanted at 78 °K, which may be compared with $E = 3.2$ J cm^{-2} required for those implanted at 300 °K. This is reasonable as the defect capture is more effective for low temperature implantation and the resulting amorphous layer is thicker.

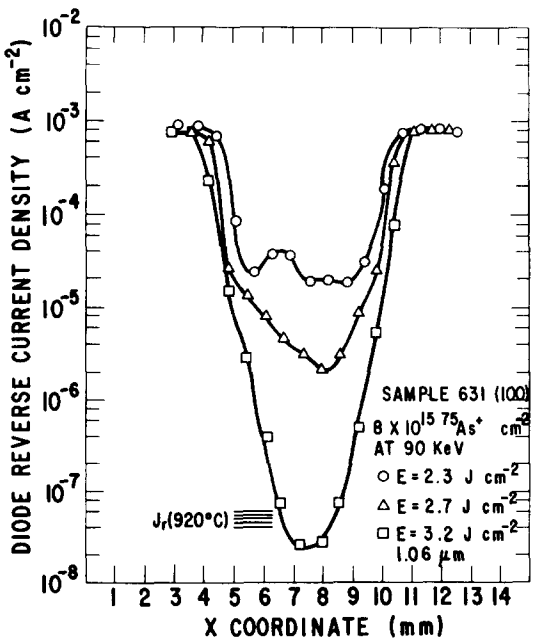

FIG. 1. Leakage current distributions for diode arrays fabricated with an ion implant of 8×10^{15} As cm^{-2} at 90 KeV and followed by laser annealing at different energy densities.

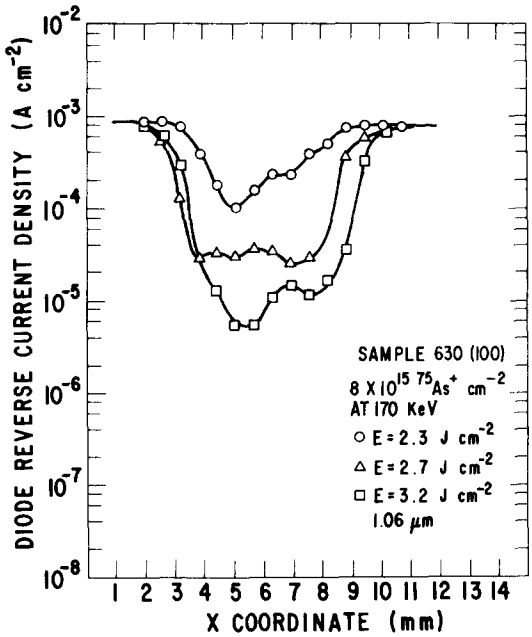

FIG. 2. Leakage current distributions for diodes fabricated from Si having a 170-KeV implant with other conditions identical to those shown in Fig. 1.

The experimental data shown previously were obtained for the diodes annealed with one-shot laser irradiation. Experiments using multiple laser pulse annealing were also carried out. Figures 3(a)–3(d) show the reverse leakage currents for the diode arrays annealed with one shot, two shots, and eight shots of laser radiation with different annealing energy densities, $E = 2.9$, 4.9, 6.3, and 7.3 J cm^{-2}, respectively. The implants were carried out with 8×10^{15} $^{75}As^{+}$ ions at 90 KeV at 78 K. For lower laser annealing energy densities, $E = 2.9$ and 4.9 J cm^{-2}, a reduction of the leakage current

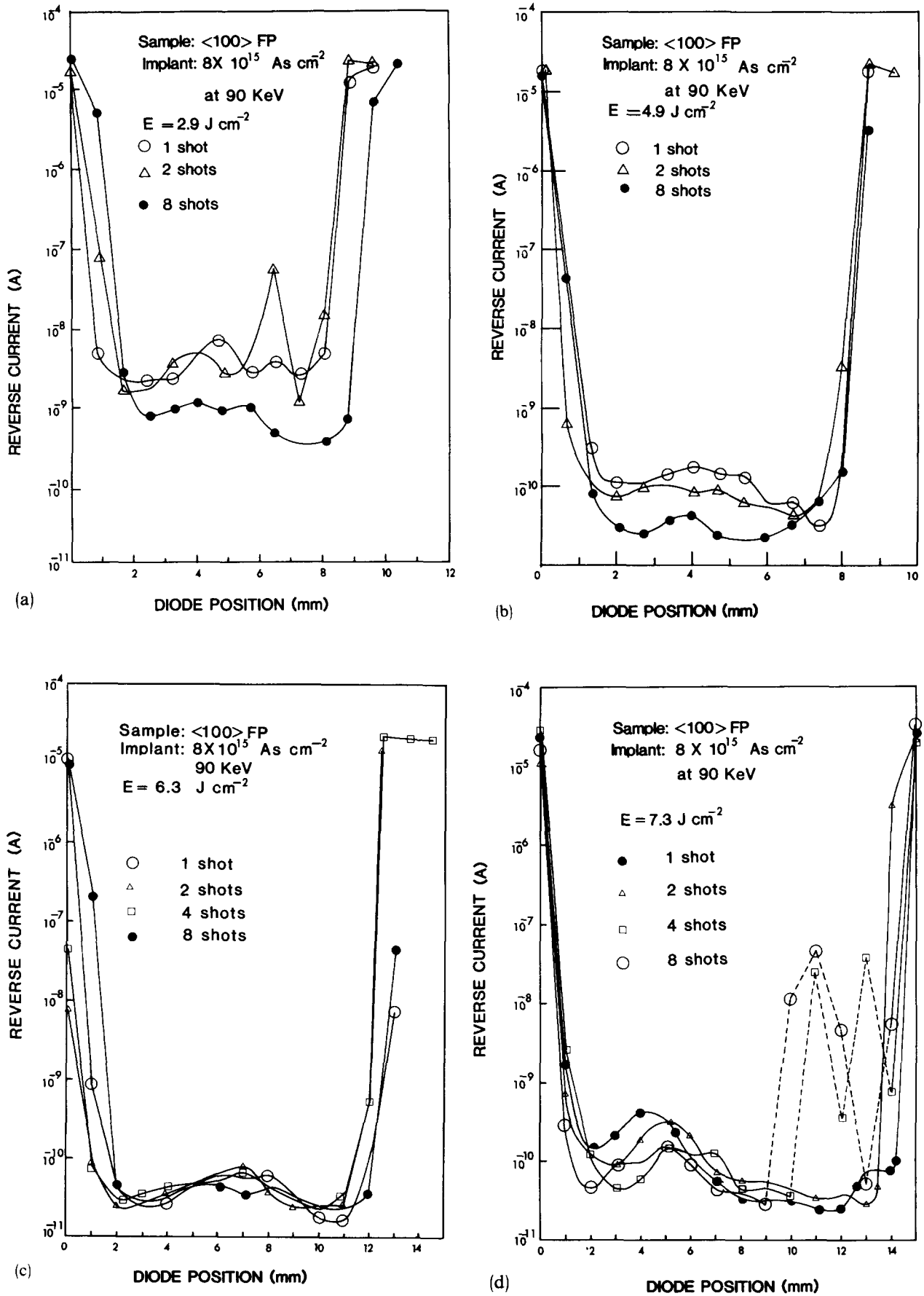

FIG. 3. Leakage current distributions for diode arrays annealed with a single and multiple shot of laser radiation having an energy density of (a) 2.9 J cm^{-2} per pulse, (b) 4.9 J cm^{-2}, (c) 6.3 J cm^{-2}, and (d) 7.3 J cm^{-2}. The implants were carried out with a fluence of 8×10^{15} As cm^{-2} at 90 KeV at 78 K.

following multiple shots was observed. On the other hand, no further reduction was achieved for those with the higher annealing energy densities. This multiple-irradiation effect is further illustrated in Fig. 4 showing the average leakage current change as a function of the number of pulses for diodes fabricated in the annealed regions.

It should be pointed out that since the repetition rate is so low (about 1–10 s^{-1}) that the substrate temperature should have approached the steady-state temperature before a subsequent shot arrived. The multiple shot annealing kinetics in general depends on the annealing energy density, repetition rate, implantation conditions and others, and is very complex. In the case of a very low repetition rate as in the present case, the melting of the amorphous layer was likely and a reduction of the leakage current was observed if the energy density is sufficiently high. For annealing with a low energy density but still above the surface melting threshold, only a fraction of the amorphous layer near the surface melts upon laser irradiation. The molten layer subsequently regrown becomes polycrystalline in most cases (it is possible to regrow as a single crystalline film if the surface is relatively undamaged).[18] Subsequent irradiations would cause the remainder of the amorphous layer to melt further into the bulk since the amorphous layer has a higher absorption coefficient than the regrown layer for the laser wavelength used $\lambda = 1.06\,\mu$m. Since the surface region was already recrystallized and became polycrystalline, the same energy density would not be sufficient to remelt the surface regrown layer.

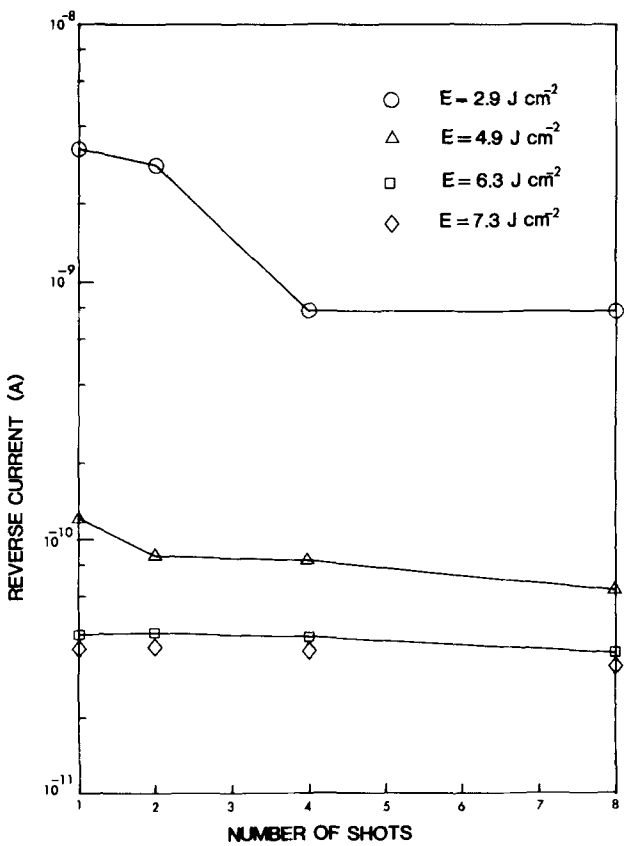

FIG. 4. Average leakage current density for diodes annealed with multiple laser irradiations.

Consequently, the multiple shots were not so effective in achieving a high quality film. For a high energy density, the situation is different and it is possible to melt entire amorphous layer and to regrow entirely from the crystalline bulk. Consequently, a high quality single crystal film can result in this case. However, liquification of the amorphous layer is not sufficient for obtaining a low diode leakage current since the tail of the ion-implanted damaged region, where point defects lie, cannot be reached by the melt front and therefore cannot be annealed. These defects may be annealed by increasing the energy density to melt Si deep into the bulk. When the energy density needed is extremely high, surface damage commonly observed can occur. The defects may also be annealed by highly repetitive multiple irradiations to thermally anneal the defects without melting or by a low-temperature furnace anneal. Multiphoton–phonon interaction can also be responsible for the multiple-shot annealing of point defects. A further discussion on point-defects distributions after annealing will be described in a subsequent section. In the case of extremely high repetition rates, the annealing kinetics approaches to solid-phase epitaxy.

The I–V characteristics of laser annealed diodes fabricated from two different substrate orientations, ⟨110⟩ and ⟨111⟩, were compared and no significant difference were observed under the same annealing conditions. Similarly, there is no observable difference in their electrical characteristics for annealing carried out in the Ar and the air ambient.[9]

B. Deep-level defects and their distributions

The fabricated diodes were investigated with deep-level transient spectroscopy (DLTS), whose detailed description may be found in other references.[20] For a p-type sample, a Si implant was performed at 300 K, with otherwise the same conditions as those described before, and the DLTS spectra were obtained after annealing with energy densities of 2.3, 2.7, and 3.2 J cm^{-2}, respectively as shown in Fig. 5. The DLTS bias conditions for the solid line spectrum were set to give majority carrier traps, or hole traps. Five observed hole trap levels are designated at $H1$ at $E_v + 0.15$ eV, $H2$ at $E_v + 0.23$ eV, $H3$ at $E_v + 0.31$ eV, $H4$ at $E_v + 0.39$ eV and $H5$ at $E_v + 0.47$ eV, and their concentrations decrease as the annealing laser energy densities increase. The reduction of the capacitance transient as the laser energy density increases from 2.7 to 3.2 J cm^{-2} is shown with a dashed and a broken line in Fig. 5. Similar defects were observed in As-implanted samples as shown in Fig. 6 with solid line. For comparison, As-implanted partially annealed diodes were forward biased to inject minority carriers, and the dashed-line spectrum of Fig. 6 revealed two additional elecron traps, $E1$ at $E_c - 0.23$ eV and $E2$ at $E_c - 0.44$ eV.[3] Since the DLTS probes mostly the lightly doped region or in this case the p-side of the p-n junction (As-implanted case) during the majority carrier trap characterization, the defects observed are the point defects near the tail of the damage profile for nearly completely annealed samples. For partially annealed samples, the point defects and other higher orders of defects of those in cluster forms were observed near the junction. These defects in the p-type substrate may be compared with

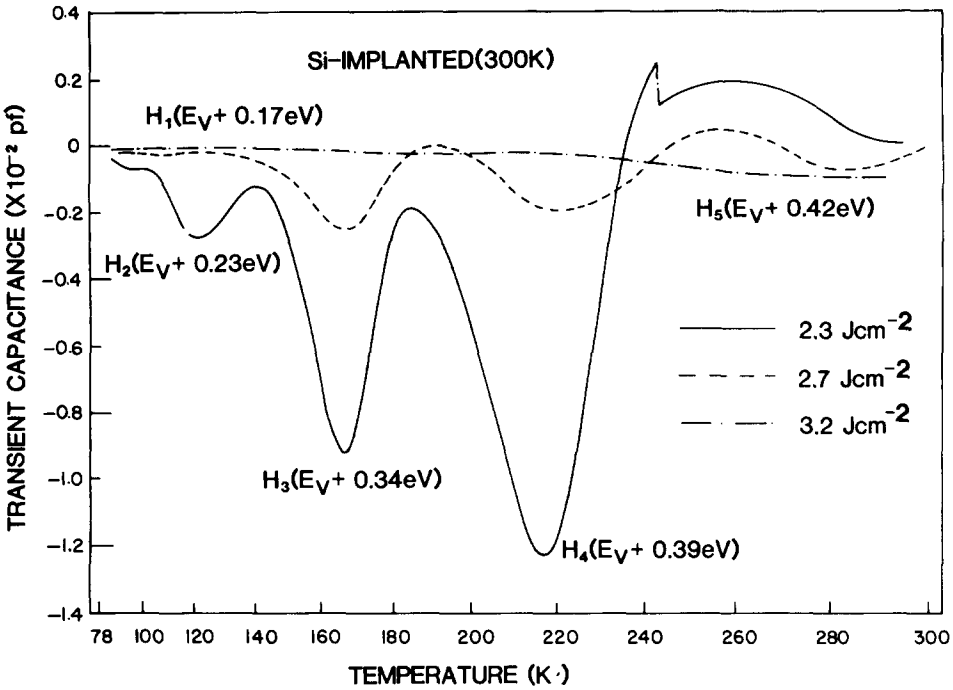

FIG. 5. DLTS spectra of the diodes laser-annealed with one shot using the energy densities as shown in Fig. 3.

those observed in high energy e-irradiated and low fluence ion-bombarded cases, in which the defect centers produced in As-irradiated p-type silicon self-anneal at room temperature to become the observed levels here. These major defects were believed to be found commonly in boron-doped samples.[2] By comparing the defects observed here to other works, the $H2$ level may be assigned to a positively charge divacancy[21–23] and the $E_v + 0.39$ eV level to a vacancy–carbon–oxygen complexes or [V + C + O]. Lee and Corbett tentatively assigned the $E_c - 0.23$ eV and $E_v + 0.31$ eV levels to an interstitial oxygen–boron complex [O_I + B] and a vacancy–oxygen–boron complex, [V + O + B] while Kimerling and others assigned the $E_c = 0.23$ eV level to a boron–boron pair [B_I + B_I].[24,25] The $E_v + 0.47$ eV level has been argued to be associated with a vacancy–boron complex [V + B].[26] On the other hand, this level is also very close to that of the iron interstitial as observed in quenched boron-doped Si.[26] In the present case of As-implantation, the heavily damaged n region, which presumably has a high concentration of vacancy–arsenic pairs [V + As] can contribute to the signal of the observed peak at $E_v + 0.47$ eV. Similarly, divacancies in the n region can contribute to the observed $H2(E_v + 0.21$ eV) level. The $E2$ level at $E_c - 0.44$ eV observed here was close to that reported by Kimerling[27] in a proton bombardment study. The level $E_v + 0.18$ eV shown in Fig. 6, was observed when the bias condition was set to probe very close to the junction and could be due to the vacancy–oxygen [V + O] pairs present in the n region. Likewise, the levels $E_v + 0.47$ eV in Fig. 6 could be due to the [V + As] pairs in the n region.

For $^{28}Si^+$ implants in n-type silicon, the DLTS spectra obtained from fabricated Schottky diodes are shown in Fig.

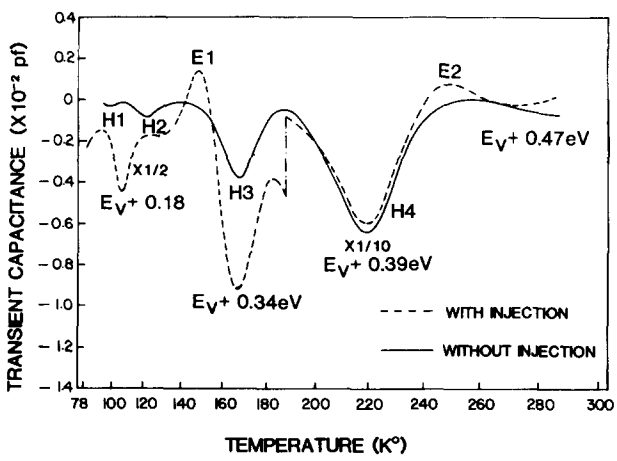

FIG. 6. Shown in solid line is the DLTS spectrum of a partially annealed sample after an As implant at 300 K. The dashed line spectrum reveals two additional electron traps $E1$ and $E2$.

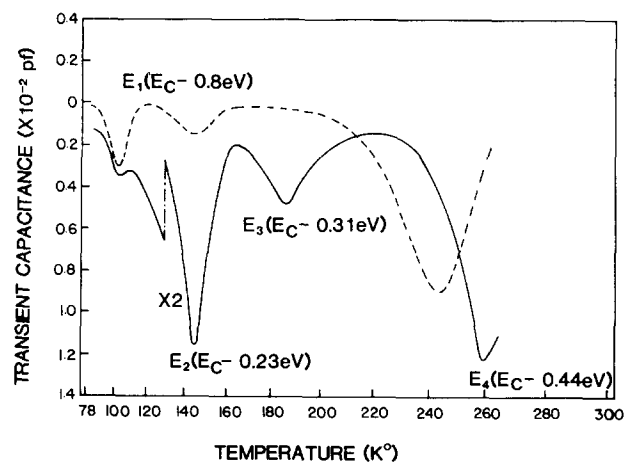

FIG. 7. DLTS spectrum for a partially annealed Si-implanted n-type sample (solid line). Also shown (dashed line) is the defect spectrum of e^- irradiated n-type Si.

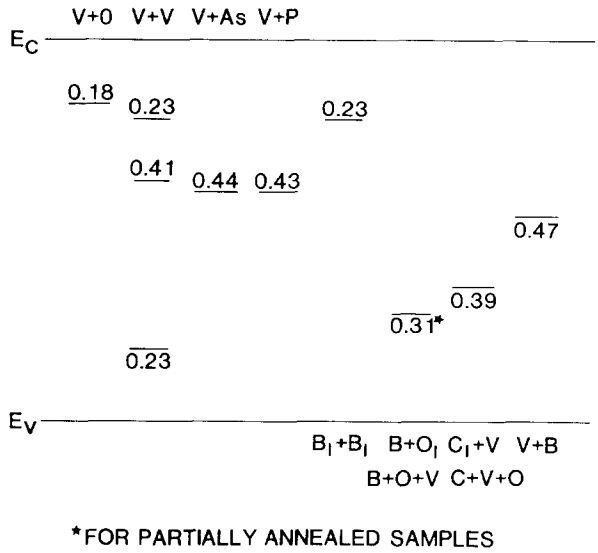

FIG. 8. Defect levels observed after pulsed laser annealing.

7, which illustrates four electron traps.

E_1 at $E_t = E_c - 0.18$ eV,

E_2 at $E_t = E_c - 0.23$ eV,

E_3 at $E_t = E_c - 0.31$ eV,

E_4 at $E_t = E_c - 0.44$ eV.

These defects again can be identified when compared with high energy electron-irradiated and low fluence ion-implanted cases shown in dashed line. The $E1$ level may be assigned to the oxygen–vacancy center, $E2$ divacancy (VV^-), $E4$ a combination of divacancy and arsenic–vacancy center.[28] The E_3 level has not been identified and may be due to a higher-order cluster. The assignments of these defects are summarized in Fig. 8.

For the ion implants carried out with the same conditions excepting the implant temperature being held at 78 K, similar defects were observed for different anealing energy densities. In Fig. 9, double peaks at near $E_v + 0.39$ eV were observed for the room temperature implant. It is believed that the second peak of the double peaks is due to a higher-order cluster. For higher annealing energy densities, the dominant distributions are expected to be different from those of the room-temperature implant. The DLTS spectra of samples exposed to multiple-shot irradiation were also obtained. A typical spectrum is shown with a double line in Fig. 9 for annealing with eight pulses using a density of 5.6 J cm^{-2} per pulse. The defect concentration decreases as the number of shots increases in agreement with the similar behavior of reverse leakage current. In addition, some changes of spectra were observed possibly due to the formation of intermediate point defects as a result of substrate heating. These centers have also been observed in thermal annealing studies of these point defects.

The defect distribution profiles are shown in Fig. 10 for samples implanted at 78 K and annealed with one shot having different energy densities. The depth was measured from the junction, which was formed after laser annealing. The junction depth increases as the melt front moves in towards the bulk with a higher annealing energy density. The defect concentrations decrease as the number of laser irradiations increase. The solid data points in Fig. 11 illustrate the major defect distributions for two samples annealed with eight shots of laser irradiation using different energy densities, $E = 2.9$ and 4.9 J cm^{-2}, respectively. The open data points shown are the same distribution for the one-shot annealing with $E = 2.9$ J cm^{-2} shown in Fig. 10, depicted here for the convenience of comparison.

In summary, the residual defect types after pulsed laser annealing are almost identical, independent of the annealing energy. The annealing mechanism of the point defects may be explained as follows. For the present case of high fluence implants there is a damaged region as shown in Fig. 12, which has largely point defects extending farther into the bulk beyond the amorphized layer. After laser irradiation

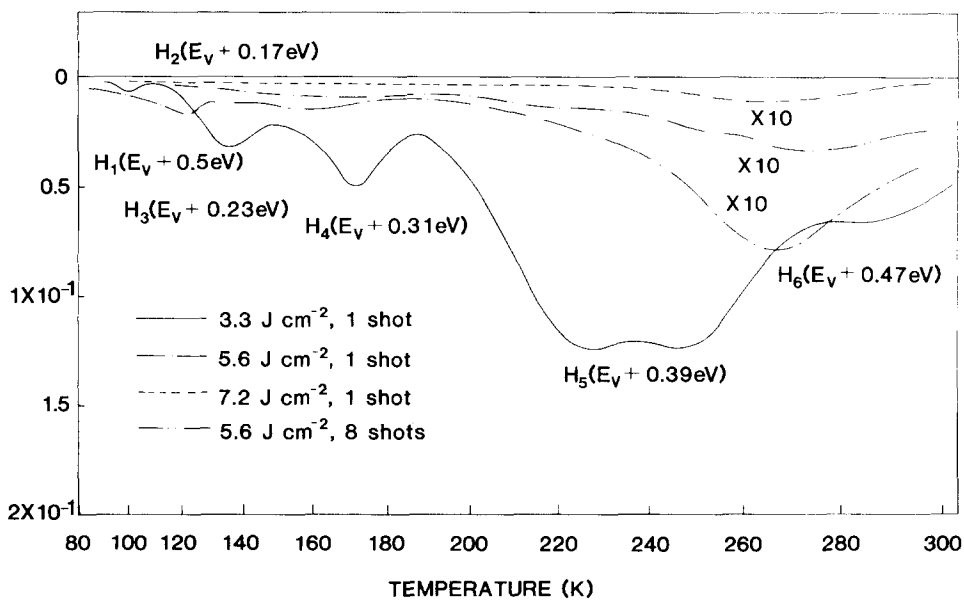

FIG. 9. DLTS spectrum for multiple shots of laser radiation.

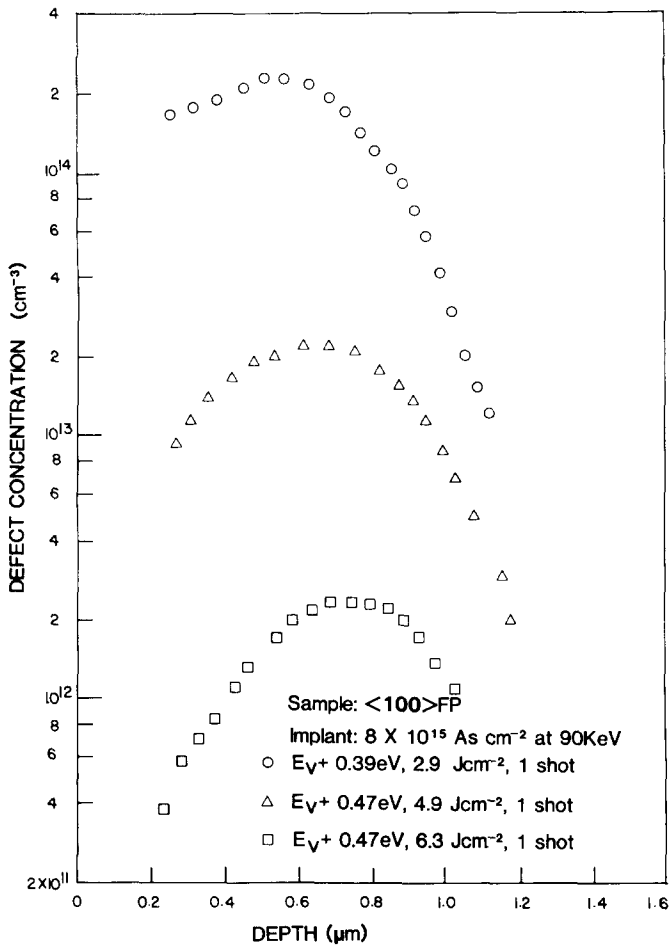

FIG. 10. Major deep-level defect distributions after annealing with energy densities of 2.9 J cm^{-2} (○), 4.9 J cm^{-2} (△) and 6.3 J cm^{-2} (□), respectively. The ion implant conditions were the same as those in Fig. 3.

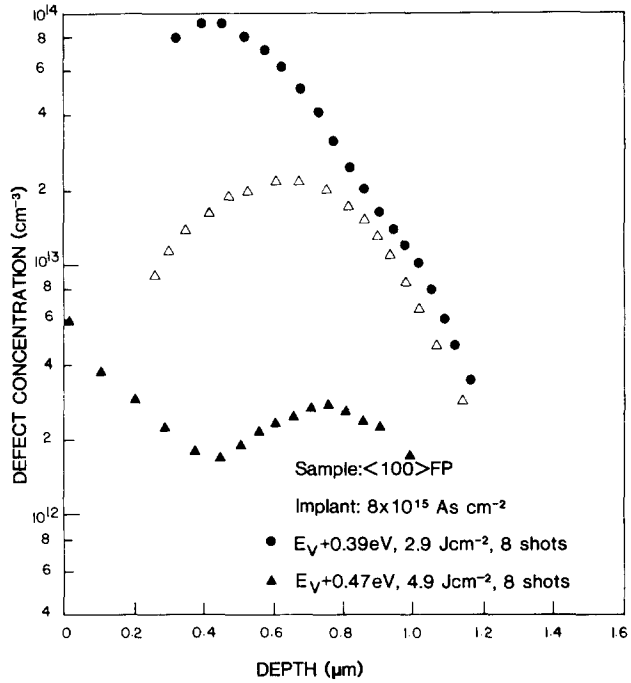

FIG. 11. Major deep-level defect distribution for annealing with multiple irradiations. The full circle data points (○) are for the $E_v + 0.39$ eV level after being annealed with eight shots of laser pulses having 2.9 J cm^{-2} per pulse while the (△) data points are for the $E_v + 0.47$ V level with eight shots and 4.9 J cm^{-2} per pulse. Also shown in (△) are data for one shot of 2.9 J cm^{-2} laser radiation for the convenience of comparison.

with an intermediate energy density, the surface melts and recrystallizes such that the junction forms in the damaged region at a depth beyond that defined by the ion implant. Since the DLTS probes largely the lightly doped p substrate region, the defects measured are likely the same kinds of point defects created by the low fluence ionic bombardment (or electron irradiation) and are situated in the tail of the damage profile. As the laser irradiation energy increases, the melt front and thus the junction move farther into the bulk. The reduction of the deep level defect concentrations in the p-side may be attributed to two mechanisms. The first mechanism is the movement of the junction into a position, where the defect concentration is lower and the second mechanism is the defect annealing due to the heating in the region beyond molten Si. The intense laser radiation produces a dose electron-hole plasma with characteristic temperature. This dense hot plasma can diffuse inward before the energy relaxes by means of phonon emission and subsequently soften the lattice.[29] Thus heating can extend beyond the molten region by means of carrier diffusion. In addtion, the dense electron-hole plasma can screen out the Coulombic trapping of vacancies and promote interstitial migration, which results in the annihilation of the point defects. This ionization enhanced diffusion has been well documented.[30]

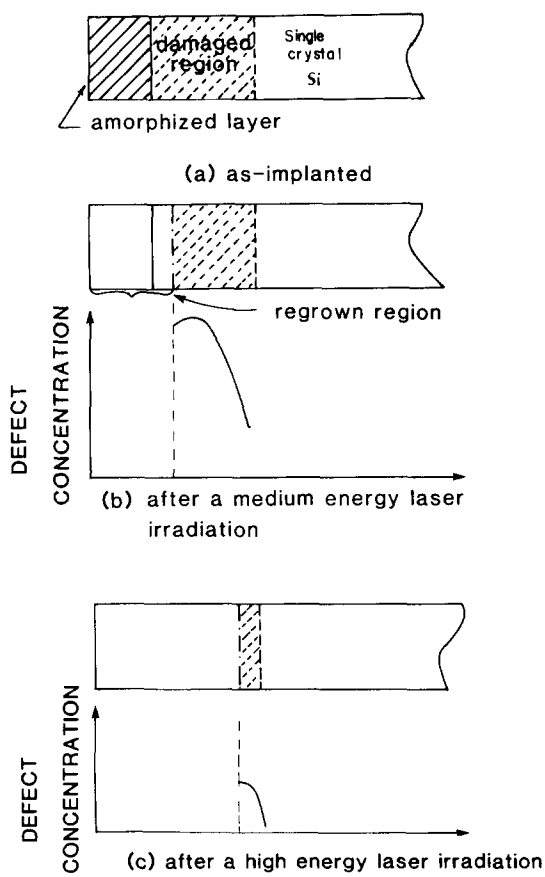

FIG. 12. Illustrating the point defect annealing mechanism for laser annealing due to the inward movement of the junction. (a) As-implanted, (b) after a medium energy laser irradiation, and (c) after a high energy laser irradiation.

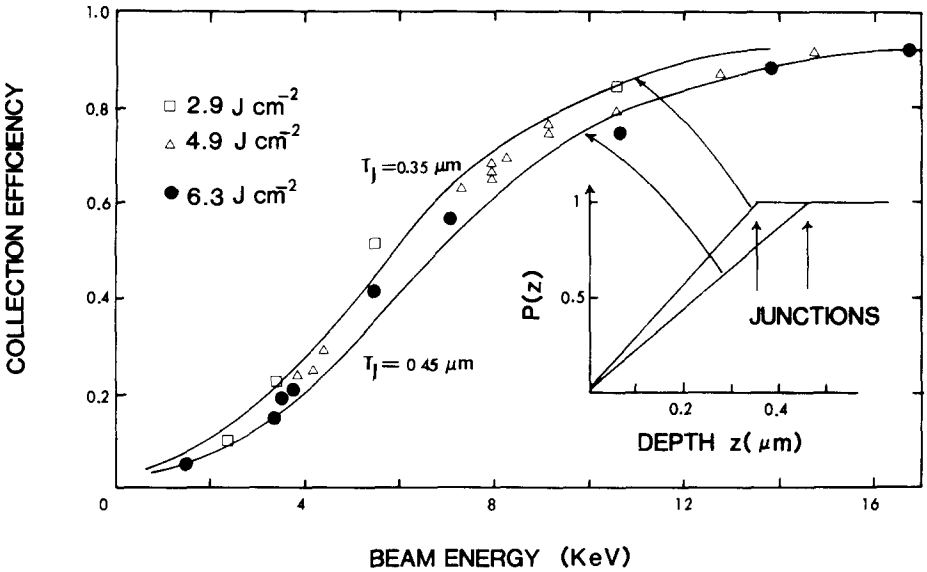

FIG. 13. EBIC collection efficiency versus beam energy for three laser annealed diodes. Solid curves are calculated collection efficiencies based on the collection probabilities shown in the inset.

These nonthermal mechanisms may be responsible for a further reduction of the defect concentration in the solid region immediately adjacent to the molten layer. As shown in Fig. 10, the decrease of the defect concentration from the sample annealed with $E = 2.9$ J cm^{-2} to the one annealed with $E = 6.3$ J cm^{-2} indicates that the junction moved in by about 0.18 μm. This was obtained by measuring the depth translation needed to have the later profile (annealed with the higher energy density) to coincide the former one. The electron beam induced conductivity study to be described later shows that the junction moved in actually only by at most 0.1 μm when the higher energy density was used.

C. Quantitative electron beam induced conductivity (QEBIC) measurements

Three of the laser annealed 78-K-implanted diodes were examined using quantitative electron beam induced conductivity (QEBIC).[31,32] This method utilizes an electron beam to generate minority carriers in the silicon. The collected fraction of the minority carrier collection probability $P(z)$ as a function of depth z was then obtained. Fig. 13 shows the QEBIC data for the three laser annealed diodes. The collection efficiency η is defined as the fraction of minority carriers collected, normalized to the number generated, including a backscattering correction. The solid curves are fits to the data using the minority carrier collection probabilities as a function of depth shown in the inset. The collection probability P can be related to the collection efficiency[31,32] by

$$\eta(\mathrm{E}) = \int_0^{1.1} P\,[qR\,(E)]\lambda\,(q)dq, \tag{1}$$

where $R\,(E)$ is the Grün range and $\lambda\,(q)$ is the normalized Grün function.[33,34] The fits shown in Fig. 13 are unique within the uncertainty due to experimental error. This uncertainty in $P(z)$ increases with depth. Near the surface for $z < 0.1$ μm the uncertainty is less than 5% in $P(z)$. The junction depth T_N is identified as the depth where $P(z) = 1$. For these samples this junction depth is uncertain by about $\pm$ 0.1 μm; however, if it is assumed that all these samples have approximately the same doping profile, then the $P(z)$ fit nearer the surface ($z < 0.2$ μm) can be used to extrapolate to the junction. Using this technique the relative differences in junction depth indicated by the fits in Fig. 13 are accurate to $\pm$ 0.05 μm although the absolute junction depths are still in error by 0.1 μm. Note that the junction depth determined by this method is for the edge of the depletion region closest to the top surface. For a substrate doping level of 2×10^{15} cm^{-3} this will be about 0.1 μm shallower than the metallurgical junction depth, depending upon the exact shape of the As doping profile near the junction.

From these measurements it can be concluded that the junction depths of the three samples increased by 0.1 μm between the 2.9-J cm^{-2} one-shot and 6.3-J cm^{-2} one-shot conditions; the 4.9-J cm^{-2} one-shot sample has a junction depth slightly less than the 6.3-J cm^{-2} one-shot diode.

The maximum sampling depth of the QEBIC technique is limited by the maximum electron range of 7 μm in this case. Since the measured collection efficiency asymptotically approached unity and did not decrease up to the highest used beam energy of 31 keV, the collection probability which best fits the data is unity between 0.5 and 5 μm. Diffusion lengths $l < 20$ μm in the substrate would be detected because $P(z)$ would have an observable $\exp(-z/l)$ dependence. Larger diffusion lengths can be measured using the lateral EBIC methods[35–38] where the signal is measured as a function of lateral distance from the junction edge. Figure 14 shows some results using this method. The beam energy was 31 keV and the results were not beam energy sensitive. If the normalized surface recombination velocity $\overline{S} = S_v l / D_n$ of the substrate surface interface is small compared to unity then the data should fit a simple exponential whose slope is determined by the diffusion length indicated. The analysis of this geometry assumes a uniform diffusion length in the substrate. These results are not controlled by the first few microns of the defect distribution tails because this region of the sample was removed during the mesa etching of the diodes. For the diffusion lengths observed here $\overline{S} = 0.1$ corresponds to $S_v = 300$ cm/sec. Larger values of S_v are quite likely for bare p-type surfaces and the EBIC data on some areas especially after prolonged electron beam irradiation exhibited

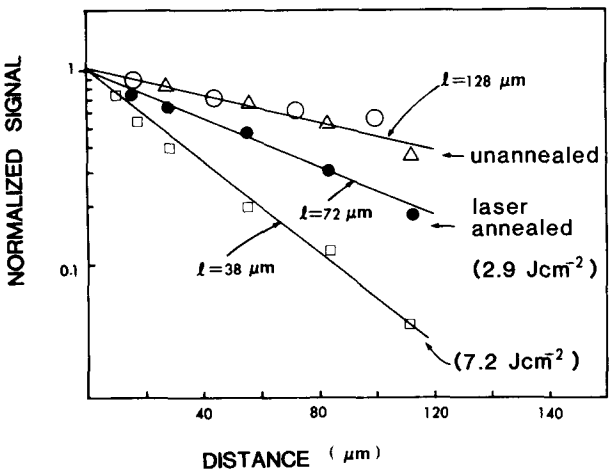

FIG. 14. Normalized EBIC signal vs lateral distance from mesa diode edge for unannealed and laser annealed diodes. Different diffusion lengths were obtained for annealed and unannealed samples.

evidence of increased S_v which depressed and distorted the simple exponential behavior. The top curve in Fig. 14 is based on data from two areas of the wafer which were not laser annealed. The unannealed As-implanted diodes had sufficient activation to permit observation of small EBIC signals. Because of this, it was possible to observe the diffusion lengths in both the annealed and unannealed portions of the wafer substrate. The unannealed substrate has a diffusion length of 128 μm while the power laser annealed region has a diffusion length of 72 μm and the higher power region 38 μm.

The shorter diffusion lengths in the annealed surface may be due to the diffusion of thermally generated defects into the substrate, due to the heating by the laser pulse, which diffuse into the substrate and are trapped by impurities, producing electrically active trapping sites.[10,15] These defects may lie many microns deep in the bulk material.

IV. CONCLUSION

In conclusion, the residual defects of the Q-switched laser annealed As-implanted p-type Si were shown to be similar to point defects found in low fluence ion-implanted or high-energy electron irradiated samples. The decrease of the defect concentrations as the laser energy density increases is in agreement with the decrease of the reverse bias leakage current of the annealed diodes. The forward bias characteristics of the diodes illustrated the quality of the regrown films. Partial melting of the amorphized layer resulted in a poor quality film, and creation of a melt front moving beyond the depth of the amorphorized layer by the use of the high laser energy density was necessary for obtaining a high quality film. From the measured defect distributions, two anneal mechanisms for the points defects were asserted: One is an apparent effect and is due to the inward movement of the melt front and the junction; the other is possibly due to the heating by the diffused electron hole plasma in the region beyond the molten Si. The QEBIC measurements confirm this finding and, in addition, the measured results of the minority carrier lifetimes using QEBIC support the assertion that complete melting is necessary for single-crystal regrowth and for obtaining a high quality film with pulsed laser annealing. Since the point defects and their behavior are the same as those introduced by high-energy electron irradiation, it is not surprising that these defects can be removed with a thermal anneal below 500 °C. Diffusion length measurements appear to suggest that there are defects that lie deep in the bulk due to diffusion of thermally generated defects, which are subsequently trapped.

[1] W. L. Brown, in *Laser and Electron-Beam Solid Interactions and Material Processing*, edited by J. F. Gibbons, L. D. Hess, and T. W. Sigmon (North-Holland, Amsterdam, 1981), p. 1.

[2] J. A. Roth, G. L. Olson, S. A. Kokorowski, and L. D. Hess, in *Laser and Electron-Beam Solid Interactions and Material Processing*, edited by J. F. Gibbons, L. D. Hess, and T. W. Sigmon (North-Holland, Amsterdam, 1981), p. 413.

[3] J. A. Van Vechten, in *Laser and Electron Beam Processing of Materials*, edited by C. W. White and P. S. Peercy (Academic, New York, 1980), p. 53.

[4] R. T. Young, C. W. White, G. J. Clark, J. Narayan, W. H. Christie, M. Murakami, P. W. King, and S. D. Kramer, Appl. Phys. Lett. **32**, 139 (1978); A. Gat., J. F. Gibbons, T. J. Magee, J. Peng, V. R. Deline, P. Williams, and C. A. Evans, Appl. Phys. Lett. **32**, 276 (1978).

[5] R. A. McMahon, H. Ahmed, and A. G. Cullis, Appl. Phys. Lett. **37**, 1016 (1980).

[6] H. J. Leamy, G. A. Rozgonyi, T. T. Sheng, and G. K. Celler, Appl. Phys. Lett. **32**, 535 (1978).

[7] A. G. Cullis, J. M. Poate, and G. K. Celler, AIP Conf. Proc. No. 50., edited by S. D. Ferris, H. J. Leamy, and J. M. Poate (American Instiute of Physics, New York, 1978), p. 311.

[8] A. V. Dvurechensky, G. A. Kachurin, T. W. Mustafin, and L. S. Smirnov, AIP Conf. Proc. No. 50., edited by S. D. Ferris, H. J. Leamy, and J. M. Poate (American Institute of Physics, New York, 1978), p. 245.

[9] L. C. Kimerling and J. L. Benton, in *Laser and Electron Beam Processing of Materials*, edited by C. W. White and P.S. Peercy (Academic, New York, 1980), p. 385.

[10] J. L. Benton, C. J. Doherty, S. D. Ferris, L. C. Kimerling, H. J. Leamy, and G. K. Celler, in *Laser and Electron Beam Processing of Material*, edited by C. W. White and P. S. Peercy (Academic, New York, 1980), p. 430; R. A. Street and N. M. Johnson, *ibid.* p. 435; K. L. Brower and P. S. Peercy, *ibid.* p. 441.

[11] N. M. Johnson, Materials Research Society Meeting, November, 1981, paper IV. 7.

[12] D. K. Biegelsen, Materials Research Society Meeting, November, 1981, paper IV. 8.

[13] K. L. Wang, Y. S. Liu, C. G. Kirkpatrick, and G. E. Possin, AIP Conf. Proc. No. 50, edited by S. D. Ferris, H. J. Leamy, and J. M. Poate (American Institute of Physics, New York, 1978), p. 569

[14] A. Mesli, E. Buttung, A. Goltzene, J. C. Muller, J. P. Ponpon, B. Meyer, C. Schwab, and P. Siffert, AIP Conf. Proc. No. 50 (1978), edited by S. D. Ferris, H. J. Leamy, and J. M. Poate (American Institute of Physics, New York, 1978), paper IV. 11

[15] N. H. Sheng, M. Mizuta, and J. L. Merz, Appl. Phys. Lett. **40**, 68 (1982)

[16] D. H. Auston, C. M. Surko, T. N. C. Venkatesan, R. E. Slusher, and J. A. Golovchenko, Appl. Phys. Lett. **33**, 437 (1978).

[17] Y. S. Liu and K. L. Wang, Appl. Phys. Lett. **34**, 363 (1979).

[18] E. Rimini, P. Baeri, S. U. Campisano, and G. Foti, AIP Conf. Proc. No. 50, p. 259, edited by S. D. Ferris, H. J. Leamy, and J. M. Poate (American Institute of Physics, New York, 1978).

[19] S. W. Chiang, Y. S. Liu, and R. F. Reihl, Appl. Phys. Lett. **39**, 752 (1981).

[20] K. L. Wang, J. Appl. Phy. **53**, 449 (1982); G. L. Miller, D. V. Land, and L. C. Kimerling, in Annu. Rev. Mater. Sci. 7, 377 (1977).

[21] P. M. Mooney, L. J. Cheng, M. Suli, J. D. Gerson, and J. W. Corbett, Phys. Rev. B **15**, 3836 (1977).

[22] J. W. Walker and C. T. Sah, Phys. Rev. B 7, 4587 (1973).

[23] J. W. Corbett and G. D. Watkins, Phys. Rev. **138A**, 555 (1965).

[24] G. D. Watkins, Phys. Rev. **12** B, 5824 (1975).

[25]G. D. Watkins, Phys. Rev. **13 B**, 2511 (1976).
[26]A. Mitic, T. Sato, H. Nishi, H. Hashimoto, Appl. Phys. Lett. **36**, 48 (1980); J. D. Gerson, L. J. Cheng, and J. W. Corbett, J. Appl. Phys. **48**, 4821 (1977).
[27]L. C. Kimerling and J. M. Poate, Inst. Phys. Conf. Ser. No. 23 (1975), p. 126.
[28]L. C. Kimerling, Inst. Phys. Conf. Ser. No. 31 (1977), p. 221.
[29]J. A. Van Vechten, in *Laser and Electron Beam Processing of Materials*, edited by C. W. White and P. S. Peercy (Academic, New York, 1980), p. 53.
[30]J. C. Bourgoin and J. W. Corbett, Radiat. Eff. **36**, 157 (1978).
[31]G. E. Possin and C. G. Kirkpatrick, in *Electron Beam Depth Profiling in Semiconductors*, Proc. SEM 1979, edited by O. Johari (Washington, D. C., March 1979), pp. 245–56.
[32]G. E. Possin and C. G. Kirkpatrick, J. Appl. Phys. **50**, 4033 (1979).
[33]A. E. Grün, Z. Naturforsch. Teil A **12**, 89 (1956).
[34]T. E. Everhart and P. H. Hoff, J. Appl. Phys. **42**, 5856 (1971).
[35]G. E. Possin and C. G. Kirkpatrick, J. Vac. Sci. Technol. **16**, 1917 (1979).
[36]W. van Roosbroeck, J. Appl. Phys. **26**, 380 (1979).
[37]F. Berz and H. K. Kuiken, Solid State Electron. **19**, 437 (1976).
[38]J. F. Bresse, *Electron Beam Induced Current in Silicon Planar p-n Junctions: Physical Model of Carrier Generation, Determination of Some Physical Parameters in Silicon*, Proc. SEM, edited by O. Johari IITRI (St. Louis, Missouri, 1972), pp. 106–112.